Epidermal growth factor receptor and *Ink4a/Arf*: Convergent mechanisms governing terminal differentiation and transformation along the neural stem cell to astrocyte axis

Robert M. Bachoo,[1,2,4,10] Elizabeth A. Maher,[1,2,10] Keith L. Ligon,[3,5] Norman E. Sharpless,[2] Suzanne S. Chan,[2] Mingjian James You,[2] Yi Tang,[7] Jessica DeFrances,[2] Elizabeth Stover,[2] Ralph Weissleder,[7] David H. Rowitch,[3] David N. Louis,[6] and Ronald A. DePinho[2,8,9]

[1]Center for Neuro-Oncology
[2]Department of Adult Oncology
[3]Department of Pediatric Oncology
Dana-Farber Cancer Institute
[4]Department of Neurology
[5]Department of Pathology
Division of Neuropathology
Brigham and Women's Hospital
[6]Department of Pathology and Neurosurgical Service
[7]Center for Molecular Imaging Research
Department of Radiology
Massachusetts General Hospital
[8]Departments of Genetics and Medicine
Harvard Medical School
Boston, Massachusetts 02115
[9]Correspondence: ron_depinho@dfci.harvard.edu
[10]These authors made equal contributions to this work.

Summary

Ink4a/Arf **inactivation and epidermal growth factor receptor (EGFR) activation are signature lesions in high-grade gliomas. How these mutations mediate the biological features of these tumors is poorly understood. Here, we demonstrate that combined loss of $p16^{INK4a}$ and $p19^{ARF}$, but not of p53, $p16^{INK4a}$, or $p19^{ARF}$, enables astrocyte dedifferentiation in response to EGFR activation. Moreover, transduction of *Ink4a/Arf*$^{-/-}$ neural stem cells (NSCs) or astrocytes with constitutively active EGFR induces a common high-grade glioma phenotype. These findings identify NSCs and astrocytes as equally permissive compartments for gliomagenesis and provide evidence that $p16^{INK4a}$ and $p19^{ARF}$ synergize to maintain terminal astrocyte differentiation. These data support the view that dysregulation of specific genetic pathways, rather than cell-of-origin, dictates the emergence and phenotype of high-grade gliomas.**

Introduction

Glioblastoma (GBM), the most common and lethal subtype of the malignant gliomas, is characterized by intense proliferation and widespread invasion of poorly differentiated cells. These highly advanced tumors can arise de novo (primary GBM) or evolve from a well-differentiated low-grade astrocytoma (secondary GBM) over a 5–10 year period (Kleihues and Cavenee, 2000), suggesting that common mechanisms drive the genesis of primary GBM and the transition to secondary GBM. Indeed, the frequent association of *Ink4a/Arf* loss of function and activation of EGFR in GBM (Ekstrand et al., 1991; Hayashi et al., 1997; von Deimling et al., 1992) raises the possibility that critical functional interactions between these mutations underlie a common mechanism of cellular transformation. The precise contributions of these mutations to the tumor phenotype are not known, although immortal growth is characteristic of *Ink4a/Arf* null murine astrocytes (Holland et al., 1998b) and replicative

SIGNIFICANCE

This work, demonstrating that both astrocytes and neural stem cells can serve as the cell-of-origin for high-grade malignant gliomas, addresses a longstanding debate in the field of neuro-oncology and neurodevelopment. The central finding is that a combination of EGF receptor pathway activation and loss of both $p16^{INK4a}$ and $p19^{ARF}$ tumor suppressor function provokes a common high-grade glioma phenotype regardless of the specific cell-of-origin. Moreover, this work identifies a new function for *Ink4a/Arf* tumor suppressor, and interaction with EGFR activation, in the maintenance of astrocyte terminal differentiation. Together, these findings provide insight into the cellular origins of malignant glioma and the role of its signature genetic lesions in the pathogenesis of these highly lethal brain cancers.

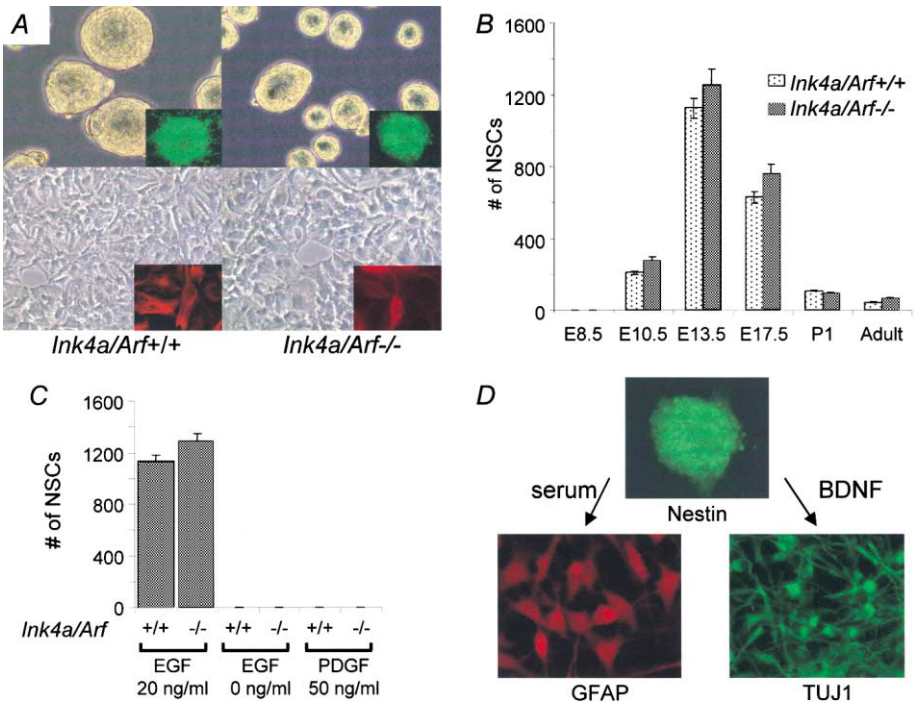

Figure 1. Comparison of *Ink4a/Arf*$^{+/+}$ and $^{-/-}$ NSCs and astrocytes

A: NSC morphology (upper panels) and nestin staining (inset upper panels) of neurospheres is similar for *Ink4a/Arf*$^{+/+}$ and $^{-/-}$ cultures. Astrocyte morphology (lower panels) and GFAP staining (inset lower panels) is also similar between *Ink4a/Arf*$^{+/+}$ and $^{-/-}$ cultures. **B:** The total number of EGF responsive NSCs isolated from *Ink4a/Arf*$^{+/+}$ and $^{-/-}$ brains at E8.5 (n = 4), E10.5 (n = 9), E13.5 (n = 38), E17.5 (n = 12), P1 (n = 16), and adult (6 weeks, n = 4). **C:** The total number of neurospheres generated in defined media with EGF (20 ng/ml), without EGF, and with PDGF (50 ng/ml). Data represent the means ± the standard error of the mean (SEM) of the number of stem cells residing in the striatal germinal zone at E13.5 (n = 32–38 embryos per genotype). **D:** Differentiation of *Ink4a/Arf*$^{-/-}$ NSCs (nestin positive) into astrocytes (GFAP positive, lower left) in response to serum and neurons (TUJ1, lower right) in response to BDNF.

senescence can be elicited upon p16^{INK4a} reintroduction into human malignant glioma cells (Uhrbom et al., 1997).

Previous work has indicated that delivery of activated EGFR into the brains of newborn *Ink4a/Arf*$^{-/-}$ mice can induce glial tumors more readily when targeted to the nestin-expressing rather than the GFAP-expressing compartment (Holland et al., 1998a). Because both NSCs and early astroglial progenitors express nestin, it has been proposed that this less mature compartment may provide a more permissive state for the transforming effects of EGFR pathway activation. Moreover, the GFAP regulatory element can drive expression into multipotent type-B cells of the subventricular zone in vivo (Doetsch et al., 1999), and cells expressing immature markers have been derived from the GFAP-expressing compartment in vitro (Holland et al., 1998b). Thus, the possible evolution of glioma from the mature astrocytic cell, as opposed to a GFAP-positive immature compartment, remains unclear in available genetic model systems. Through the use of rigorously defined primary NSC and mature astrocyte cultures, the present study sought to determine whether the specific state of glial cell differentiation plays a restrictive role in glioma progression or, alternatively, whether glioma relevant mutations can alter the state of differen-

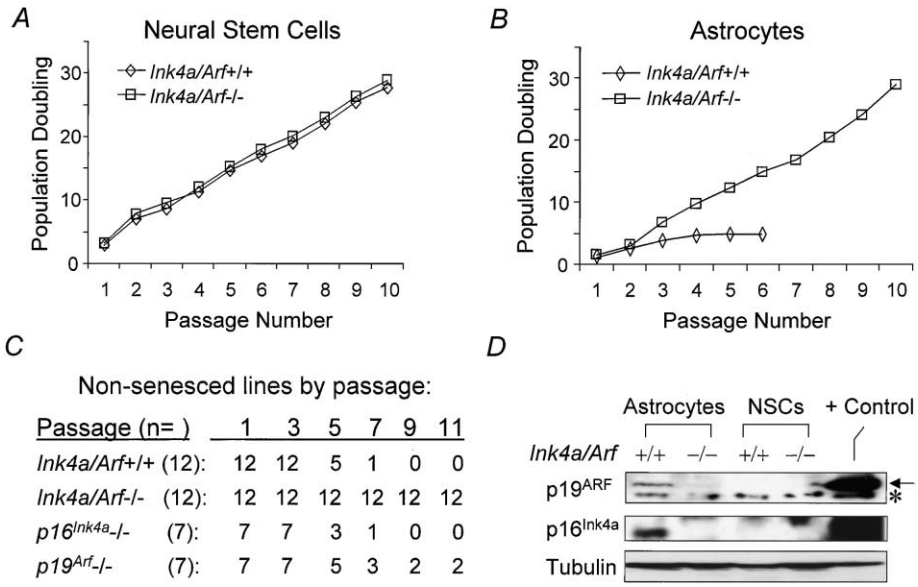

Figure 2. p16^{INK4a} and p19^{ARF} cooperate to regulate the growth of astrocytes but not NSCs

Growth during serial passage by *Ink4a/Arf* genotype for NSCs (**A**) and astrocytes (**B**). **C:** Number of persistently growing astrocyte lines (i.e., "non-senesced" [Sharpless et al., 2001]) by passage and p16^{INK4a} and p19^{ARF} status. **D:** Western blot analysis of p16^{INK4a} and p19^{ARF} in NSCs and astrocytes by *Ink4a/Arf* genotype. +Control = p16^{INK4a} and p19^{ARF} overexpressing tumor cell line.

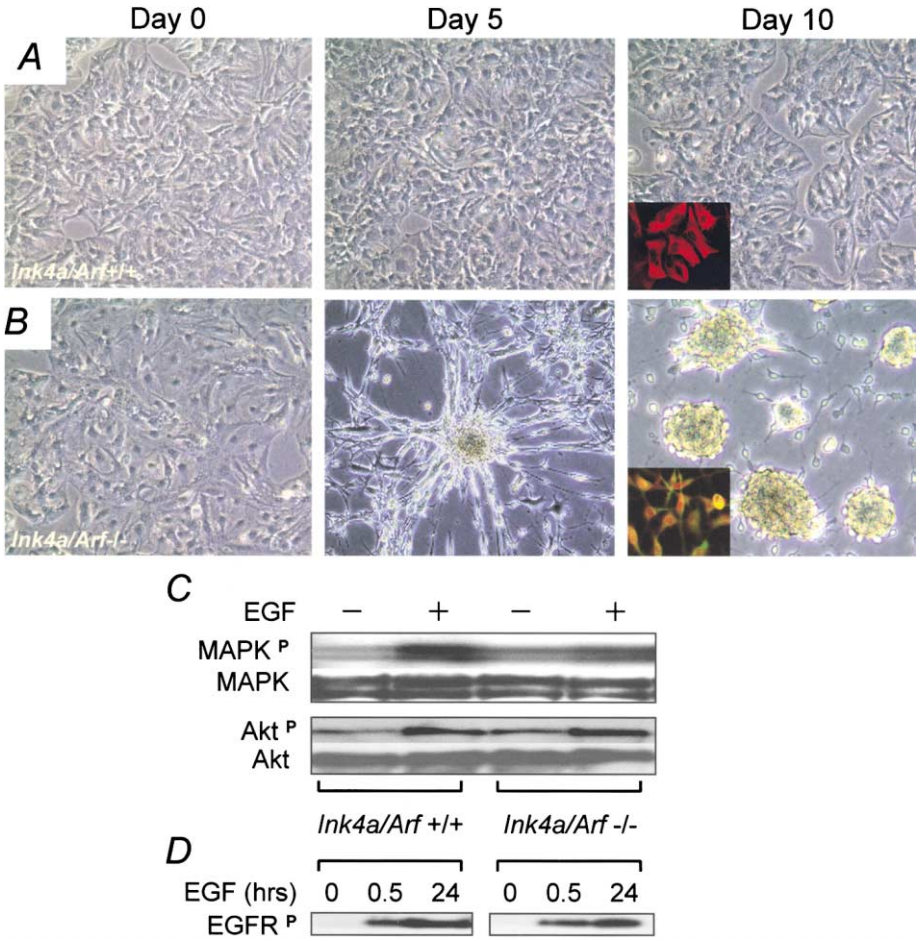

Figure 3. Ink4a/Arf$^{-/-}$ astrocytes dedifferentiate to nestin^{+}, A2B5^{+} progenitor cells in vitro

Ink4a/Arf$^{+/+}$ (**A**) and $^{-/-}$ (**B**) cells were removed from serum and grown in EGF on day 0. *Ink4a/Arf*$^{-/-}$ cells rapidly change morphology and resulting bipolar cells and neurospheres are nestin^{+} and A2B5^{+} (double labeling inset, far right panel of **B**), whereas *Ink4a/Arf*$^{+/+}$ cells do not dedifferentiate and remain GFAP^{+} (inset, far right panel of **A**). Western blot analysis of cultured astrocytes of indicated genotypes after treatment with EGF. Equivalent MAPK and AKT (**C**), and EGFR (**D**), phosphorylation is seen in *Ink4a/Arf*$^{-/-}$ and $^{+/+}$ cells after EGF exposure.

tiation and dictate the tumor phenotype regardless of the cell-of-origin.

Results

Previous gross and histological analyses of *Ink4a/Arf*$^{-/-}$ mice are consistent with normal central nervous system structure and function (Serrano et al., 1996 and R.M.B. and R.A.D., unpublished). In this study, the dispensability of p16^{INK4a} and p19^{ARF} function in brain development was confirmed by an extensive histological and morphometric analysis of the developing brain from *Ink4a/Arf*$^{-/-}$ mutants and control littermates on embryonic days E13.5, E15.5, and E19, postnatal days 1 and 25, and aging adults (data not shown). These studies were complemented by a series of cell culture-based analyses of the growth and differentiation of NSCs and cortical astrocytes. The various *Ink4a/Arf* genotypes exhibited similar morphology and differentiation markers of primary NSC and astrocyte cultures (Figure 1A) and showed comparable emergence of an EGF-responsive NSC pool on E10.5, with expansion through E13.5 (Figure 1B)—kinetics that reflect the increased EGF responsiveness during development (Chiasson et al., 1999; Qian et al., 2000). Similar to littermate wild-type cultures, *Ink4a/Arf*$^{-/-}$ NSCs retained strict EGF dependence for growth, and PDGF substitution was unable to sustain wild-type or mutant cultures (Figure 1C). Moreover, *Ink4a/Arf* status did not affect the capacity of NSCs to differentiate into GFAP-positive astrocytes (93 $\pm$ 4%) and TUJ1-positive neurons (40 $\pm$ 5%) in response to serum and BDNF, respectively (Figure 1D).

The established cell-type specific roles of p16^{INK4a} and p19^{ARF} in cellular growth control (Kamijo et al., 1999; Randle et al., 2001; Sharpless et al., 2001) prompted a detailed proliferation analysis of early passage NSC and astrocyte cultures. Although *Ink4a/Arf*$^{+/+}$ and $^{-/-}$ NSCs (Figure 2A) exhibited comparable growth rates, there was a striking increase in the proliferative rate of *Ink4a/Arf*$^{-/-}$ astrocytes relative to wild-type cultures (Figure 2B). Correspondingly, cell cycle analysis of early passage astrocyte cultures showed marked differences in the S phase fraction (33% for *Ink4a/Arf*$^{-/-}$ versus 12% for $^{+/+}$ astrocytes, $n = 5$ cultures each, $p < 0.005$). As shown previously for oligodendrocyte precursors (Tang et al., 2001), *Ink4a/Arf*$^{+/+}$ NSCs proliferated indefinitely if prevented from differentiating. In contrast, serially passaged *Ink4a/Arf*$^{-/-}$ astrocytes exhibited immortal growth, while *Ink4a/Arf*$^{+/+}$ astrocytes, as well as those specifically deficient for *p16*^{INK4a} (Sharpless et al., 2001) or *p19*^{ARF} (N.E.S. and R.A.D., unpublished data), underwent proliferative arrest and assumed senescent features by 5 to 7 population doublings (Figure 2C). *p19*$^{ARF-/-}$, but not *p16*$^{INK4a-/-}$ or *Ink4a/Arf*$^{+/+}$, cultures exhibited a moderate rate of escape from senescence (2 of 7 cultures, Figure 2C), while 100% of *Ink4a/Arf*$^{-/-}$ cultures were immortal. Consistent with these observed developmental stage-specific differences in cell growth control,

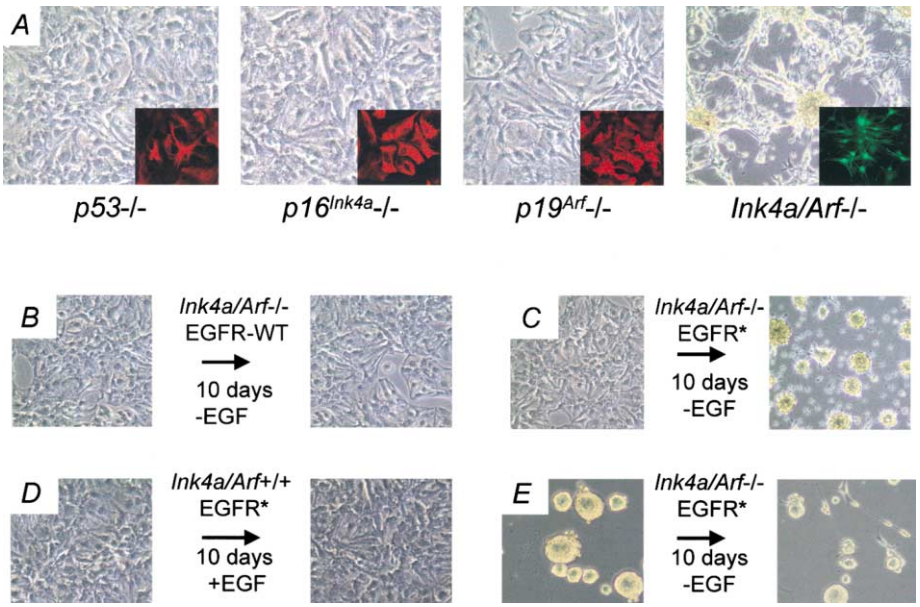

Figure 4. *p53*$^{-/-}$, *p16*$^{INK4a-/-}$, and *p19*$^{ARF-/-}$ astrocytes do not dedifferentiate in response to EGF

Cultures were grown in serum-free media supplemented with EGF (20 ng/ml) for 10 days. **A:** In contrast to *Ink4a/Arf*$^{-/-}$ astrocytes, *p53*$^{-/-}$, *p16*$^{INK4a-/-}$, and *p19*$^{ARF-/-}$ astrocytes did not change morphology in response to EGF and remained GFAP^{+} and nestin^{-} (insets represent double labeling with GFAP [red] and nestin [green] [n = 4 independently derived cell lines for each genotype]). **B:** *Ink4a/Arf*$^{-/-}$ astrocytes expressing the wild-type EGFR do not dedifferentiate in serum-free media lacking EGF. **C:** *Ink4a/Arf*$^{-/-}$ astrocytes expressing EGFR* dedifferentiate in serum-free media lacking EGF. **D:** *Ink4a/Arf*$^{+/+}$ astrocytes expressing EGFR* do not dedifferentiate. **E:** EGFR* expression in NSCs can substitute for ligand. *Ink4a/Arf*$^{-/-}$ EGFR* NSC cultures were grown in serum free media without EGF. *Ink4a/Arf*$^{-/-}$ cultures transduced with the wild-type EGFR do not proliferate under these conditions, but rather undergo apoptosis (not shown).

p16^{INK4a} and p19^{ARF} were undetectable in extensively passaged wild-type NSC cultures, whereas both p16^{INK4a} and p19^{ARF} were readily detected in cultured *Ink4a/Arf*$^{+/+}$ astrocytes (Figure 2D). Taken together, these data demonstrate that both p16^{INK4a} and p19^{ARF} play important, yet developmentally restricted, roles in the control of astroglial lineage proliferation in vitro.

The transition to a poorly differentiated glial phenotype in progression from low-grade astrocytoma to secondary GBM prompted an assessment of *Ink4a/Arf* and the EGFR pathway interactions in the maintenance of astrocyte differentiation. Subconfluent cycling early passage GFAP^{+} primary astrocytes were removed from serum-supplemented media and exposed to serum-free media containing EGF (20 ng/ml). Under these conditions, all *Ink4a/Arf*$^{+/+}$ cultures as well as astrocyte cultures derived from *p16*^{INK4a} null and *p19*^{ARF} null mice survived, continued to proliferate**,** and retained the morphological and immunohistochemical features of fully differentiated astrocytes (Figure 3A). In sharp contrast, EGF-treated *Ink4a/Arf*$^{-/-}$ astrocytes en masse showed contracted cytoplasm within 24 hr and, over the course of 7 to 10 days, developed into bipolar cells coexisting with small neurospheres which detached from the culture dish and continued to proliferate as substrate-independent neurospheres (Figure 3B)—properties ascribed to NSCs. While littermate wild-type astrocyte cultures retained GFAP expression in EGF (Figure 3A, inset), *Ink4a/Arf*$^{-/-}$ cultures demonstrated synchronous complete loss of GFAP and induction of the progenitor markers nestin and A2B5 (Figure 3B, inset). As added confirmation of the immature state, dedifferentiated cultures rapidly redifferentiated into GFAP positive astrocytes when reexposed to serum. In a small minority of cultures, TUJ1 positive neurons could be generated from the dedifferentiated astrocytes upon exposure to BDNF (data not shown). These *Ink4a/Arf*-dependent responses were not related to differences in EGFR expression or activation, as evidenced by a comparable degree of EGF-induced EGFR phosphorylation (Figure 3D) and activation of the EGFR signaling surrogates, MAPK and AKT (Figure 3C). To understand further these synergistic actions, we asked whether immortalization per se or the capacity for rapid proliferation represent the key parameters that endow EGF-induced astrocyte plasticity. Despite rapid rates of growth and an immortal phenotype, *p53*$^{-/-}$ astrocyte cultures subjected to prolonged EGF treatment failed to induce morphological or immunohistochemical changes consistent with dedifferentiation (Figure 4A). Likewise, astrocytes from mice singly deficient for either *p16*^{INK4a} or *p19*^{ARF} did not dedifferentiate in response to EGF (Figure 4A). Furthermore, in contrast to a previous report showing PDGF induction of glial progenitor morphology and expression markers in wild-type astrocytes after extended passage in culture (40 days) (Dai et al., 2001), the placement of early-passage *Ink4a/Arf*$^{-/-}$, *p53*$^{-/-}$, or *Ink4a/Arf*$^{+/+}$ astrocyte cultures in serum-free media containing 50 ng/ml PDGF did not induce dedifferentiation (data not shown); see Discussion.

To determine whether cell-autonomous effects of this glioma-relevant lesion could induce astrocyte dedifferentiation in vitro, *Ink4a/Arf*$^{+/+}$ and $^{-/-}$ astrocytes were inoculated with retrovirus encoding EGFR* or wild-type EGFR (EGFR-WT) in serum-free media with EGF supplementation. Comparable expression of transduced EGFR* and EGFR-WT protein was documented by Western blot analysis (not shown). Both EGFR* and EGFR-WT *Ink4a/Arf*$^{-/-}$ astrocytes recapitulated the aforementioned dedifferentiation response (n = 4 cultures each), although this response required EGF supplementation in the case of EGFR-WT *Ink4a/Arf*$^{-/-}$ cultures (Figures 4B and 4C). EGF− and EGFR*

Table 1. Growth of orthotopically transplanted astrocytes and NSCs in SCID brains

	Transduced with:	
	EGFR WT	EGFR*
Ink4a/arf$^{+/+}$ Astrocytes	0/4	0/4
Ink4a/arf$^{-/-}$ Astrocytes	0/4	4/4
Ink4a/arf$^{+/+}$ NSCs	0/6	0/6
Ink4a/arf$^{-/-}$ NSCs	0/6	6/6

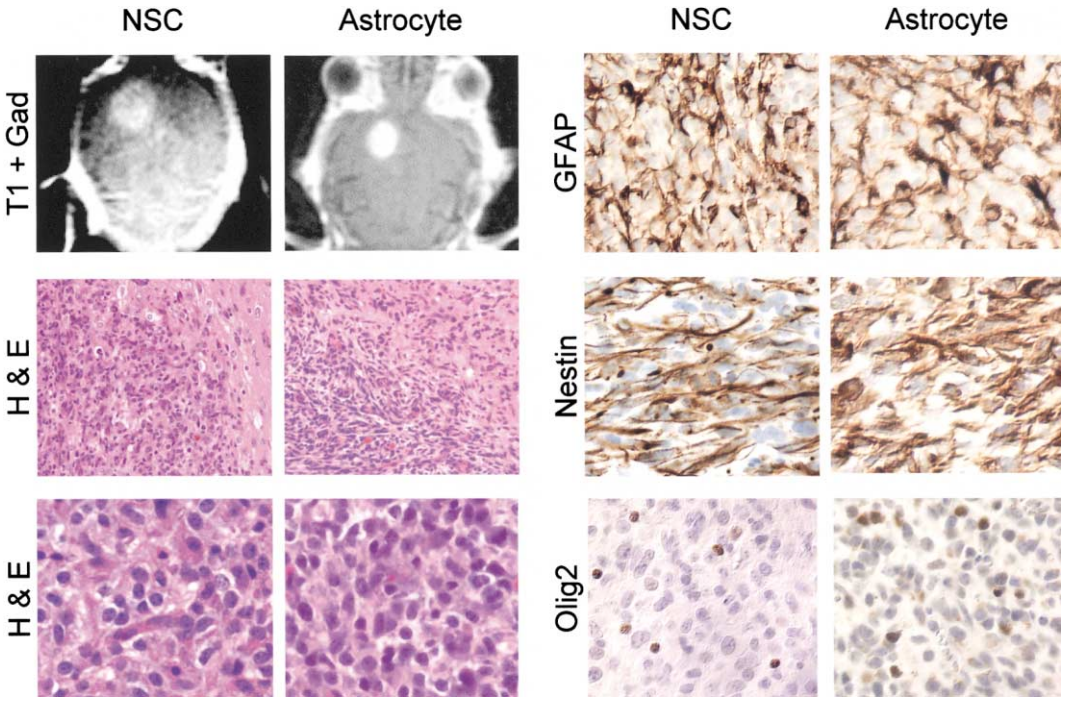

Figure 5. Expression of EGFR* in *Ink4a/Arf*$^{-/-}$ NSCs and astrocytes induces high-grade gliomas

Tumors derived from *Ink4a/Arf*$^{-/-}$ EGFR* NSCs and astrocytes orthotopically transplanted into the brain are gadolinium enhancing on MRI, grow as poorly differentiated high-grade tumors (H&E 10× and 40×), and express GFAP, Nestin, and Olig2.

induced dedifferentiation responses were similar, except that the kinetics of dedifferentiation were faster in response to EGF (average of 8.5 versus 18 days, n = 6 cultures each)—a finding consistent with a more modest activation of MAPK activation by EGFR*. Of note, despite robust and comparable levels of transduced EGFR* or EGFR-WT and activation of MAPK in EGF, *Ink4a/Arf*$^{+/+}$ cultures did not dedifferentiate under any conditions (Figure 4D, n = 4 cultures each). That EGFR* was functionally activated was documented further by the survival of dedifferentiated *Ink4a/Arf*$^{-/-}$ EGFR* cultures and *Ink4a/Arf*$^{-/-}$ EGFR* NSCs in the absence of EGF supplementation (Figure 4E). The findings corroborate the EGF ligand studies and raise the possibility that these key glioma lesions may drive the classical poorly differentiated glial phenotype of these cancers.

The genetically defined primary cultures described in this study provided an opportunity to assess directly how the state of astroglial differentiation influences the transforming actions of EGFR* in vivo. To this end, early passage EGFR* or EGFR-WT transduced NSCs (2×10^4 cells per injection, n = 6 per genotype) and astrocytes (2×10^4 cells per injection, n = 4 per genotype) from *Ink4a/Arf*$^{-/-}$ and $^{+/+}$ mice were transplanted orthotopically into the brains of adult SCID mice and followed for 12 weeks or until development of focal neurological deficits (Table 1). Astrocyte cultures were maintained in serum prior to injection to avoid the possibility that tumor formation was a result of in vitro dedifferentiation. Cultures grown for 10 days or more in serum-containing medium did not show any evidence of dedifferentiation either morphologically or immunohistochemically, regardless of EGFR and *Ink4a/Arf* status. Specifically, cultures showed GFAP immunoreactivity but remained negative for the early glial markers, nestin and A2B5 (data not shown). Moreover, it is highly unlikely that such astrocyte cultures would be contaminated with NSCs since primary cultures were derived from P5 cortex, which lacks immature cells. Neither *Ink4a/Arf*$^{+/+}$ NSCs nor astrocytes yielded tumors or neurological deficits after 3 months, even when engineered to express EGFR* (or EGFR-WT) (Table 1). In contrast, EGFR* *Ink4a/Arf*$^{-/-}$ NSC and astrocyte cultures readily formed tumors with a latency of 4–8 weeks (Figure 5). Clonality of these tumors was confirmed by the emergence of a distinct banding pattern on Southern blots assayed for hybridization to a Moloney LTR fragment when compared to parental cell lines (data not shown). The tumorigenic competence of EGFR* *Ink4a/Arf*$^{-/-}$ NSCs and astrocytes, as opposed to EGFR* *Ink4a/Arf*$^{+/+}$ controls, was documented further by tumor formation following subcutaneous injections into SCID mice (Figure 6B).

Notably, despite being at opposite ends of the differentiation spectrum, both EGFR* *Ink4a/Arf*$^{-/-}$ NSCs and astrocytes (Figure 5) yielded neoplasms with overlapping clinical, radiographic, and histopathological features. Clinically, all animals presented with focal neurological signs that included asymmetric hindlimb and forelimb dystonia followed by progressive paraplegia. These symptoms matched precisely MRI findings of gadolinium enhancing mass lesions in the striatum and did not reflect neurological trauma associated with the injection (Figure 5). Histologically, the tumors from both EGFR* *Ink4a/Arf*$^{-/-}$ NSCs and astrocytes resembled high-grade gliomas demonstrating hypercellularity, pleomorphism, high mitotic activity, and focal invasion into normal parenchyma. Five tumors derived from NSCs and 3 tumors derived from astrocytes were composed of small, undifferentiated cells (Figure 5), while 1 tumor derived from NSCs was composed of spindle-shaped cells and 1 tumor de-

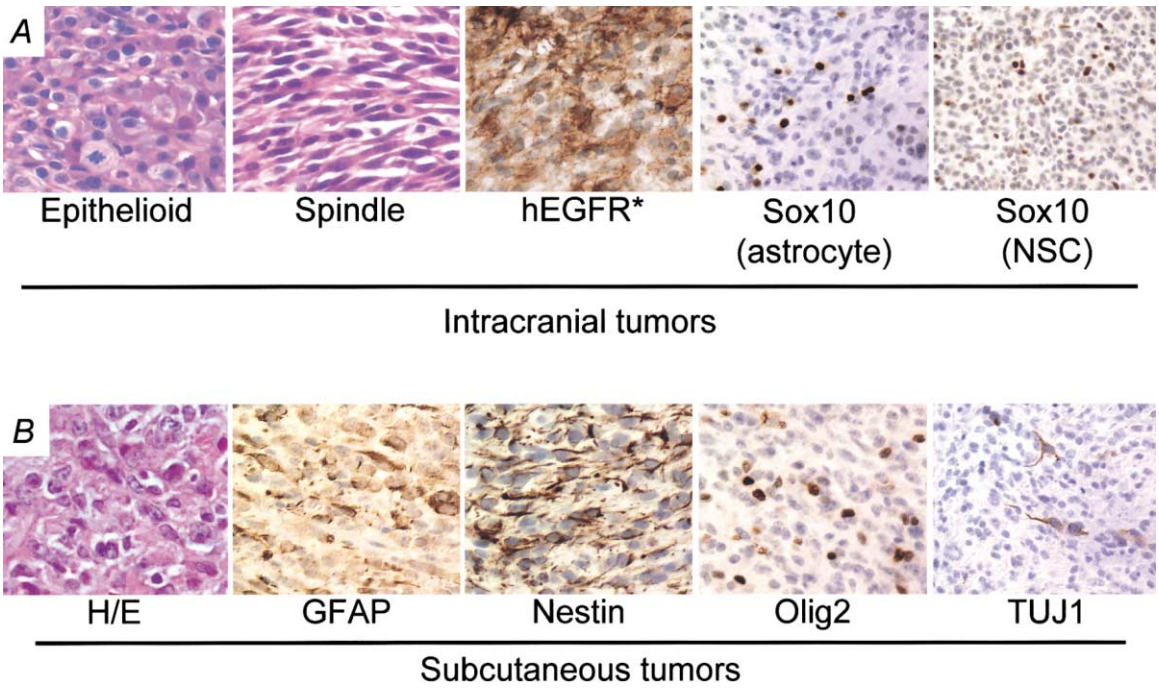

Figure 6. "Multiforme" nature of tumor cells and immunoreactivity for oligodendroglial and neuronal markers suggest dedifferentiation of astrocytes to a multipotent progenitor

A: Spindle-cell and epithelioid-cell morphology was seen in 1 tumor each derived from NSCs and astrocytes. All tumors demonstrated strong hEGFR* staining and were Sox10 positive. **B:** Subcutaneous tumors derived from *Ink4a/Arf*$^{-/-}$ astrocytes transduced with EGFR* were high grade, poorly differentiated GFAP^{+}, nestin^{+}, and Olig2^{+} tumors, similar to intracranially generated tumors. In addition, rare TUJ1 staining was observed. Similar histology and immunoreactivity to GFAP, nestin, and Olig2 were found in subcutaneous tumors derived from *Ink4a/Arf*$^{-/-}$ NSCs transduced with EGFR* (not shown).

rived from astrocytes was composed of epithelioid cells (Figure 6A). This range of cellular morphologies is consistent with the "multiforme" nature of human high-grade gliomas. Further evidence for a heterogeneous composition of glial tumors was provided by immunohistochemical analysis. EGFR*-transduced NSCs or astrocytes yielded tumors that were GFAP positive (Figure 5). In addition, we observed that all tumors expressed the immature marker nestin as well as Olig2 (Figure 5), a marker of oligodendroglial progenitors during normal development that is also expressed in human gliomas (Lu et al., 2001; Marie et al., 2001). Sox10 positive cells were components of the tumors (Figure 6A), further emphasizing the oligodendroglial composition (Zhou et al., 2000). Finally, occasional cells staining with the immature neuronal marker, TUJ1, were observed in the subcutaneous tumors derived from astrocytes (Figure 6B). These findings demonstrate that tumor cells derived from mature *Ink4a/Arf* deficient astrocytes can give rise to cells of the oligodendroglial and, rarely, neuronal lineage, thus providing strong evidence that astrocytes dedifferentiated during tumorigenesis.

To provide in vivo confirmation of the functional interrelationship between EGFR activation and the status of *Ink4a/Arf*, *Ink4a/Arf* $^{+/+}$ and $^{-/-}$ adult mice underwent intraventricular infusion of EGF for 7 days. In the setting of *Ink4a/Arf* deficiency, EGF infusion induced a marked increase in proliferation (Ki-67 $>$ 10%) and diffuse infiltration of a population of GFAP immunoreactive cells (Figure 7). These small cells with hyperchromatic nuclei formed a multilayered cuff around the ventricle and extended into the surrounding neuropil in a diffuse manner. In addition, there was conspicuous growth along white matter tracts, a pattern of spread that is typical of human gliomas. Moreover, clusters of GFAP positive tumor cells were identified in the subarachnoid space (Figure 7; lower right panel, yellow bar), further confirming that the GFAP positivity reflects expression of GFAP by tumor cells rather than background neuropil. Tumor cells stained positively with nestin- and Olig2 (Lu et al., 2001; Marie et al., 2001), with nestin positivity displayed as elongated cellular processes seen characteristically in human gliomas (Figure 7). Notably, the lesions induced in this model were cytologically and immunohistochemically similar to the tumors generated by orthotopic transplantation of astrocytes and NSCs. Moreover, EGF infusion in either *p16*^{INK4a} or *p19*^{ARF} alone induced a proliferative response of similar magnitude and degree of invasion as seen in *Ink4a/Arf*$^{+/+}$ brain (data not shown), demonstrating cooperativity between p16^{INK4a} and p19^{ARF} in this process. Together, these in vivo data serve to validate the genotypic-phenotypic correlates established in the cell culture based studies.

Discussion

We have demonstrated that NSCs and astrocytes can serve equally as the glioma cell-of-origin in the setting of *Ink4a/Arf* deficiency and constitutive EGFR activation. These data extend previous findings by clearly identifying the gliomagenic potential of these two rigorously defined compartments. However, with

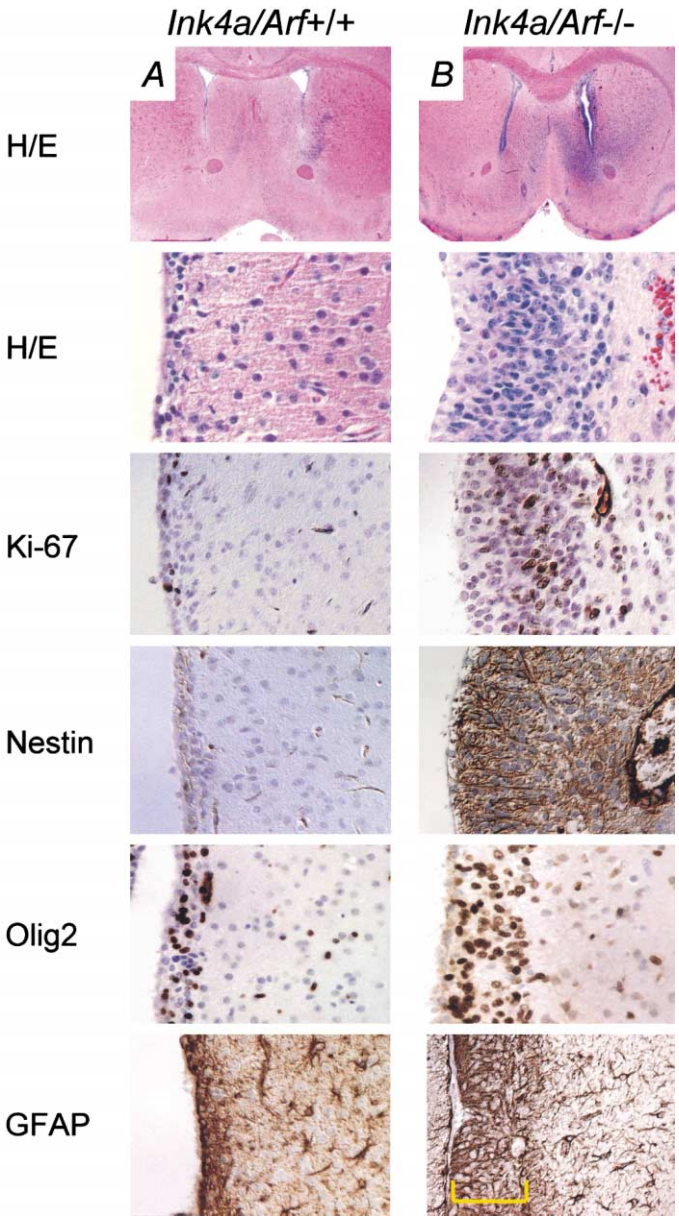

Figure 7. EGF infusion induces a marked increase in proliferation of poorly differentiated GFAP, Nestin, and Olig2 positive cells in the subventricular zone

Low and high power H&E, Ki-67, GFAP, Nestin, and Olig2 staining of *Ink4a/Arf* $^{+/+}$ (**A**) and $^{-/-}$ (**B**) mice after 7 days of intraventricular EGF infusion. Yellow bracket (bottom right panel) indicates growth of tumor cells in the subarachnoid space.

regard to previous studies, it is worth noting that GFAP, although an established astrocyte marker, has also been shown to be present in pluripotent stem cells of the subventricular zone and present in the early astrocytic progenitors (Doetsch et al., 1999; Malatesta et al., 2000). Thus, the overlapping specificities of GFAP and nestin in developing glia have made challenging the investigational efforts to identify the glioma cell-of-origin, and the identification of glial-specific promoters remains an important unmet need for modeling of gliomagenesis in a lineage-restricted fashion in vivo.

The present study clearly demonstrates that astrocytes undergo dedifferentiation to a multipotent progenitor cell during tumorigenesis, a response directly resulting from the cooperation between Ink4a/Arf deficiency and EGF signaling. Since neither *p16*^{INK4a} nor *p19*^{ARF} loss alone induced astrocyte immortalization or dedifferentiation in response to EGF in vitro, our data demonstrate a role for both proteins encoded by the *Ink4a/Arf* locus in gliomagenesis and are consistent with the dual inactivation of p16^{INK4a} and p14^{ARF} in 50%–70% of human high-grade gliomas (James et al., 1988; Labuhn et al., 2001). Although the status of the p14^{ARF}-p53 pathway is often not known in such cases, point mutations and promoter methylation affecting only p16^{INK4a} have been documented (Costello et al., 1996; Herman et al., 1995). Likewise, an inherited germline mutation affecting p14^{ARF} but not p16^{INK4a} has been associated with familial astrocytoma (Randerson-Moor et al., 2001), and mice lacking only p19^{ARF} with intact p16^{INK4a} develop spontaneous gliomas (Kamijo et al., 1997). These data are consistent with our observations and suggest that both p16^{INK4a} and p14^{ARF} play independent roles in suppressing glial tumor formation in humans.

How these pathways interact to maintain an astrocyte in a terminally differentiated state is unclear. The increase in astrocyte proliferation in response to loss of both proteins is not sufficient for dedifferentiation, since neither *Ink4a/Arf*$^{-/-}$ astrocytes in serum nor *p53*$^{-/-}$ astrocytes in EGF dedifferentiate. Although there is no evidence that p16^{INK4a} and p14^{ARF} are involved in maintaining astrocytes in a fully differentiated state in the normal brain, it is tempting to speculate that they may become important in regulating the response to oncogenic stimuli, such as EGFR activation. Indeed, the generation of poorly differentiated tumors from Ink4a/Arf deficient astrocytes expressing EGFR* supports an important role for p16^{INK4a} and p19^{ARF} in constraining dedifferentiation. The identification of both Sox10, an oligodendroglial marker (Zhou et al., 2000), and GFAP, an astrocyte marker, in the tumors is evidence for mixed glial composition, suggesting that the extent of astrocyte dedifferentiation was significant, to a cell with at least a bipotent state. The identification of rare TUJ1 positive cells suggests that dedifferentiation may be so complete as to generate a pluripotent cell with the potential to make neurons as well as glia. These data are highly consistent with human high-grade gliomas that similarly have a mixed GFAP and Olig2 staining pattern (Lu et al., 2001). Furthermore, the identification of human tumors with mixed oligodendroglial and astrocytic features may reflect the dynamic state between a fully dedifferentiated cell and the commitment to astrocyte and oligodendrocyte lineages. It is highly unlikely that expression of these lineage-restricted markers, especially 2 markers of oligodendrocyte development, simply represents aberrant gene expression in cultured astrocytes, since the same marker expression pattern was observed in tumors derived from cultured NSCs. Furthermore, lesions with similar histopathologic and immunohistochemical characteristics were generated by the intraventricular infusion of EGF in Ink4a/Arf deficient mice. Additional markers for glial tumor characterization may emerge from a more thorough understanding of glial ontogeny. Moreover, identification of regulatory elements from such markers may provide a means to specifically target subpopulations of tumor cells in vivo.

It is worth noting that the genetic patterns observed in human tumors are consistent with the biological impact documented in this study. Specifically, the cooperation between

Ink4a/Arf deficiency and EGFR overexpression in processes of dedifferentiation and generation of high-grade gliomas matches well with the high frequency of these lesions in GBM (Ekstrand et al., 1991). In contrast, lack of dedifferentiation of p53 deficient astrocytes when stimulated by EGF or PDGF in defined media is consistent with the finding that p53 deficient low-grade astrocytomas maintain a well differentiated morphology and remain GFAP positive and Olig2 negative (Lu et al., 2001). Moreover, these data reinforce the view of the specific and cooperative nature of the interactions between the EGFR pathway and *Ink4a/Arf* function in processes of astrocyte dedifferentiation.

Together, these observations provide insights into the origins, evolution, and pathophysiology of GBM and into the roles and interactions of three signature lesions, EGFR activation and loss of $p16^{INK4a}$ and $p14^{ARF}$. The data presented here serve to reconcile the seemingly distinct cellular origins of these tumors by providing evidence that the biological behavior of the high-grade gliomas depends not on the glial state of differentiation, but rather on the dysregulation of specific genetic elements.

Experimental procedures

Morphometric analysis of cerebral cortex and cell counts

Five coronal brain sections per animal were evaluated at 500 μm intervals from 0.5 to −2.00 with respect to Bregma according to a stereotaxis atlas of the mouse brain (Franklin and Paxinos, 1997). The thickness of the S2 somatosensory cortex as well as the horizontal distance from left to right corpus callosum at mid dorsal to ventral level were measured. To estimate the number of astrocytes in the brain, GFAP positive cells were counted in every tenth section (5 μm) under a 20× objective. For the cerebral cortex, the regions containing motor and somatosensory cortex were chosen; for the hippocampus, the number of GFAP positive cells under 20× in an area covering the CA1 and the dentate gyrus was chosen.

NSC and astrocyte culture techniques

Primary NSCs were isolated from the brain subventricular zone of E13.5 embryos as described (Reynolds and Weiss, 1992). Single cells were cultured in DMEM/F12 containing insulin/transferrin (Gibco), Penicillin/Streptomycin (Gibco), and EGF (Gibco, 20 ng/ml). Primary neurospheres were passaged by dissociation of the spheres into single cells using trituration through a fire polished pipette. Neurospheres were differentiated into secondary astrocytes by growth in 10% FBS in the media and into neurons by growth in defined media containing brain derived growth factor (BDNF, 50 ng/ml) (Reynolds and Weiss, 1996). Primary astrocytes were isolated from 5 day old pups and prepared according to published methods (McCarthy and de Vellis, 1980). Cells were maintained in DMEM containing 10% FBS (GIBCO). In serial passage experiments of astrocytes and NSCs, cells were seeded at 900,000 cells per dish in 10 cm plates, and then split, counted, and reseeded every 5 days. Population doubling per passage was determined as $\log_2$ (cells counted after 5 days in culture/cells seeded). Both primary and secondary astrocytes were analyzed for immortalization and dedifferentiation, but no difference was noted between cells from either source, and results were pooled in this analysis. The time course of dedifferentiation was determined by measuring the progressive change in morphology of the cells from flat polygonal cells to final culture containing bipolar cells and neurospheres. Six independently derived cultures of each genotype were studied in the dedifferentiation experiments.

Retroviral vVector and constructs

PLGIP vector was kindly provided by Dr. J.Z. Zhang (The University of Kentucky, Lexington, KY). We modified the vector by replacing the *gfp* gene with the polylinker (BamHI-Eco109I) of pBlueScript SK II (Stratagene, CA), designated as pMJ709. EGFR or the constitutively active mutant (vIIEGFR, lacking the exons 2–7), designated hereafter as EGFR*, was kindly provided by Dr. Webster Cavenee. To construct retroviruses expressing EGFR* or WT human EGFR, cDNA inserts were excised from tetop-EGFR*-KS or pPCIBA-hEGFR (H. Nakagawa, Univ. of Pennsylvania), respectively, and inserted into the BamHI-NotI sites.

Production of retrovirus stock

293T cells (4–6 × 10^6) were plated onto 10 cm dishes 14–18 hr before the transfection. Transfection by Lipofectamine Plus (Invitrogen) was performed according to the manufacturer's protocol. The retroviral supernatant was harvested 36–48 hr posttransfection and used to infect target cells. Inoculated cells were selected with 2 μg/ml Puromycin for 4 days.

Stereotactic injection of cell lines

Cells for injection were suspended in Hanks Buffered Salt Solution (10,000 cells/ul) and placed on ice. Six week old SCID mice were anesthetized with ketamine (60 mg/kg) and xylazine (7.5 mg/kg) and placed in the stereotactic frame using ear bars. A hole was bored in the skull 0.5 mm anterior and 3.0 mm lateral to the Bregma. Two μl of the cell suspension was injected into the right caudate nucleus 3–5 mm below the surface of the brain using a 26 gauge needle. The scalp was closed with 5.0 silk suture. Animals were followed daily for development of neurological deficits.

Magnetic resonance imaging

Mice with neurological deficits were anesthetized with ketamine and xylazine, as above. MR imaging was performed with a 1.5-T superconducting magnet (Signa 5.0; GE Medical Systems, Milwaukee, WI) by using a 1.5-inch surface coil. Conventional T1-weighted (300/11, repetition time msec/echo time msec), T2-weighted (2,000/102) spin-echo images were obtained in axial, coronal, and sagittal directions. The section thickness was 1.5 mm, with a field of view of 6 cm^2, a 256 × 256 matrix, yielding a spatial resolution of 234×234×1500 microns. Gd-DTPA (Magnevist: Gadopentetate dimeglumine, Shering, Berlin, Germany) enhanced T1-weighted images were obtained 5 min after tail vein injection of 10 μl of Magnevist.

Brain sectioning, pathological analysis, and immunohistochemistry

For pathological analysis, brains were fixed in 10% formaldehyde for 12 hr and processed for hematoxylin and eosin (H&E) by standard techniques. The entire brain was sectioned in 1–2 mm coronal blocks and submitted in one cassette for paraffin embedding to facilitate analysis of the whole brain. For immunohistochemical analysis, sections were prepared for staining with nestin (Pharmingen), GFAP (DAKO), Olig2 (Takebayashi), and Sox10 (Rowitch) by standard techniques. For immunohistochemical analysis of cells in culture, cells were fixed in 4% paraformaldehyde for 1 hr at 4° and stained with nestin, GFAP, and A2B5 (Chemicon) according to standard protocols.

Western blotting

Protein lysates from NSCs and astrocytes (1–2 × 10^6) were prepared as previously described (Sharpless et al., 2001). 40 μg of lysate were resolved on 4%–12% polyacrylamide gels (Novex) in MOPS buffer. Membranes were blotted for $p16^{INK4a}$, $p19^{ARF}$, tubulin as described (Sharpless et al., 2001). Other antibodies used (Santa Cruz) included EGFR, EGFR-phospho, Akt, phospho-Akt, MAPK, and phospho MAPK at dilutions recommended by manufacturers.

Implantation of miniosmotic pumps into mouse brain

EGF was unilaterally infused directly into the lateral ventricles (coordinates 4.0 mm anterior to the lambda suture, 0.7 mm lateral of midline, and 2.5 mm below the dura) using a miniosmotic pump (Model #1007, Alza, Palo Alto, CA) attached to a 30 gauge cannula. EGF was infused for 7 consecutive days at a flow rate of 0.5 μl/hr with an initial pump concentration of 33 μg/ml in 0.9% saline containing 1 mg/ml mouse serum albumin (Sigma, St. Louis, MO).

Acknowledgments

We wish to thank W. Cavenee, F. Furnari, H. Fine, H. Takebayashi, and H. Nakagawa for advice and reagents, and L. Chin for critical reading of the manuscript. This work was supported by grants from the National Institutes of Health, American Cancer Society, The Brain Tumor Association, The Multiple Sclerosis Society, The V Foundation, The Mahoney Center for Neuro-Oncology, and the Dana-Farber/Harvard Cancer Center (P30) Pilot

Project Development Award. D.H.R. is a Kimmel Scholar. R.A.D. is an American Cancer Society Research Professor.

Received: February 22, 2002
Revised: April 4, 2002

References

Chiasson, B., Tropepe, V., Morshead, C., and van der Kooy, D. (1999). Adult mammalian forebrain ependymal and subependymal cells demonstrate proliferative potential, but only subendymal cells have neural stem cell characteristics. J. Neurosci. *19*, 4462–4471.

Costello, J.F., Berger, M.S., Huang, H.S., and Cavenee, W.K. (1996). Silencing of p16/CDKN2 expression in human gliomas by methylation and chromatin condensation. Cancer Res. *56*, 2405–2410.

Dai, C., Celestino, J.C., Okada, Y., Louis, D.N., Fuller, G.N., and Holland, E.C. (2001). PDGF autocrine stimulation dedifferentiates cultured astrocytes and induces oligodendrogliomas and oligoastrocytomas from neural progenitors and astrocytes in vivo. Genes Dev. *15*, 1913–1925.

Doetsch, F., Caille, I., Lim, D.A., Garcia-Verdugo, J.M., and Alvarez-Buylla, A. (1999). Subventricular zone astrocytes are neural stem cells in the adult mammalian brain. Cell *97*, 703–716.

Ekstrand, A.J., James, C.D., Cavenee, W.K., Seliger, B., Pettersson, R.F., and Collins, V.P. (1991). Genes for epidermal growth factor receptor, transforming growth factor alpha, and epidermal growth factor and their expression in human gliomas in vivo. Cancer Res. *51*, 2164–2172.

Franklin, K.B.J., and Paxinos, G. (1997). The Mouse Brain In Stereotaxic Coordinates (San Diego, Academic Press).

Hayashi, Y., Ueki, K., Waha, A., Wiestler, O., Louis, D., and von Deimling, A. (1997). Association of EGFR gene amplification and CDKN2 (p16/MTS1) gene deletion in glioblastoma multiforme. Brain Pathol. *7*, 871–875.

Herman, J.G., Merlo, A., Mao, L., Lapidus, R.G., Issa, J.P., Davidson, N.E., Sidransky, D., and Baylin, S.B. (1995). Inactivation of the CDKN2/p16/MTS1 gene is frequently associated with aberrant DNA methylation in all common human cancers. Cancer Res. *55*, 4525–4530.

Holland, E., Hively, W., DePinho, R.A., and Varmus, H. (1998a). A constitutively active epidermal growth factor receptor cooperates with disruption of G1 cell-cycle arrest pathways to induce glioma-like lesions in mice. Genes Dev. *112*, 3675–3685.

Holland, E.C., Hively, W.P., Gallo, V., and Varmus, H.E. (1998b). Modeling mutations in the G1 arrest pathway in human gliomas: overexpression of CDK4 but not loss of INK4a-ARF induces hyperploidy in cultured mouse astrocytes. Genes Dev. *12*, 3644–3649.

James, C.D., Carlbom, E., Dumanski, J.P., Hansen, M., Nordenskjold, M., Collins, V.P., and Cavenee, W.K. (1988). Clonal genomic alterations in glioma malignancy stages. Cancer Res. *48*, 5546–5551.

Kamijo, T., Bodner, S., van de Kamp, E., Randle, D.H., and Sherr, C.J. (1999). Tumor spectrum in ARF-deficient mice. Cancer Res. *59*, 2217–2222.

Kamijo, T., Zindy, F., Roussel, M.F., Quelle, D.E., Downing, J.R., Ashmun, R.A., Grosveld, G., and Sherr, C.J. (1997). Tumor suppression at the mouse INK4a locus mediated by the alternative reading frame product p19ARF. Cell *91*, 649–659.

Kleihues, P., and Cavenee, W.K. (2000). World Health Organization Classification of Tumours of the Nervous System (Lyon: IARC Press).

Labuhn, M., Jones, G., Speel, E.J., Maier, D., Zweifel, C., Gratzl, O., Van Meir, E.G., Hegi, M.E., and Merlo, A. (2001). Quantitative real-time PCR does not show selective targeting of p14(ARF) but concomitant inactivation of both p16(INK4A) and p14(ARF) in 105 human primary gliomas. Oncogene *20*, 1103–1109.

Lu, Q.R., Park, J.K., Noll, E., Chan, J.A., Alberta, J., Yuk, D., Alzamora, M.G., Louis, D.N., Stiles, C.D., Rowitch, D.H., and Black, P.M. (2001). Oligodendrocyte lineage genes (OLIG) as molecular markers for human glial brain tumors. Proc. Natl. Acad. Sci. USA *98*, 10851–10856.

Malatesta, P., Hartfuss, E., and Gotz, M. (2000). Isolation of radial glial cells by fluorescent-activated cell sorting reveals a neuronal lineage. Development *127*, 5253–5263.

Marie, Y., Sanson, M., Mokhtari, K., Leuraud, P., Kujas, M., Delattre, J.Y., Poirier, J., Zalc, B., and Hoang-Xuan, K. (2001). OLIG2 as a specific marker of oligodendroglial tumour cells. Lancet *358*, 298–300.

McCarthy, K.D., and de Vellis, J. (1980). Preparation of separate astroglial and oligodendroglial cell cultures from rat cerebral tissue. J. Cell Biol. *85*, 890–902.

Qian, X., Shen, Q., Goderie, S.K., He, W., Capela, A., Davis, A.A., and Temple, S. (2000). Timing of CNS cell generation: a programmed sequence of neuron and glial cell production from isolated murine cortical stem cells. Neuron *28*, 69–80.

Randerson-Moor, J.A., Harland, M., Williams, S., Cuthbert-Heavens, D., Sheridan, E., Aveyard, J., Sibley, K., Whitaker, L., Knowles, M., Newton Bishop, J., and Bishop, D.T. (2001). A germline deletion of p14(ARF) but not CDKN2A in a melanoma-neural system tumour syndrome family. Hum. Mol. Genet. *10*, 55–62.

Randle, D.H., Zindy, F., Sherr, C.J., and Roussel, M.F. (2001). Differential effects of p19(Arf) and p16(Ink4a) loss on senescence of murine bone marrow-derived preB cells and macrophages. Proc. Natl. Acad. Sci. USA *98*, 9654–9659.

Reynolds, B.A., and Weiss, S. (1992). Generation of neurons and astrocytes from isolated cells in the central nervous system. Science *255*, 1707–1710.

Reynolds, B.A., and Weiss, S. (1996). Clonal and population analyses demonstrate that an EGF-responsive mammalian embryonic CNS precursor is a stem cell. Dev. Biol. *175*, 1–13.

Serrano, M., Lee, H., Chin, L., Cordon-Cardo, C., Beach, D., and DePinho, R.A. (1996). Role of the INK4a locus in tumor suppression and cell mortality. Cell *85*, 27–37.

Sharpless, N.E., Bardeesy, N., Lee, K.H., Carrasco, D., Castrillon, D.H., Aguirre, A.J., Wu, E.A., Horner, J.W., and DePinho, R.A. (2001). Loss of p16Ink4a with retention of p19Arf predisposes mice to tumorigenesis. Nature *413*, 86–91.

Tang, D.G., Tokumoto, Y.M., Apperly, J.A., Lloyd, A.C., and Raff, M.C. (2001). Lack of replicative senescence in cultured rat oligodendrocyte precursor cells. Science *291*, 868–871.

Uhrbom, L., Nister, M., and Westermark, B. (1997). Induction of senescence in human malignant glioma cells by p16INK4A. Oncogene *15*, 505–514.

von Deimling, A., Louis, D.N., von Ammon, K., Petersen, I., Hoell, T., Chung, R.Y., Martuza, R.L., Schoenfeld, D.A., Yasargil, M.G., Wiestler, O.D., et al. (1992). Association of epidermal growth factor receptor gene amplification with loss of chromosome 10 in human glioblastoma multiforme. J. Neurosurg. *77*, 295–301.

Zhou, Q., Wang, S., and Anderson, D.J. (2000). Identification of a novel family of oligodendrocyte lineage-specific basic helix-loop-helix transcription factors. Neuron *25*, 331–343.